Spatio-temporally reconfigurable light in degenerate laser cavities

A. Bartolo,[1,2] N. Vigne,[2], M. Marconi,[1] G. Beaudoin,[3] L. Le Gratiet,[3] K. Pantzas,[3] I. Sagnes,[3] A. Garnache,[2] and M. Giudici[1,*]

[1]*Université Côte d'Azur, CNRS, Institut de Physique de Nice, 06200 Nice, France*
[2]*Institut d'Electronique et des Systèmes, CNRS UMR5214, 34000 Montpellier, France*
[3]*Centre de Nanosciences et de Nanotechnologies, CNRS UMR 9001, Université Paris-Saclay, 91120 Palaiseau, France*
[4]*Departament de Física, Universitat de les Illes Baleares, C/Valldemossa km 7.5, 07122 Mallorca, Spain*
[5]*Institute for Theoretical Physics, University of Münster, Wilhelm-Klemm-Str. 9, 48149 Münster, Germany*
[*]*massimo.giudici@inphyni.cnrs.fr*

Abstract: We show that a III-V semiconductor Vertical External-Cavity Surface-Emitting Lasers (VECSELs) can be engineered to generate light with a customizable spatio-temporal structure. The temporal control is achieved through the emission of Temporal Localized Structures (TLSs), a particular mode-locking regime that allows the individual addressing of the pulses traveling back and forth in the cavity. The spatial profile control relies on a degenerate external cavity and it is implemented thanks to an absorptive mask deposited onto the gain mirror that limits the positive net gain within two circular spots in the transverse section of the VECSEL. We show that each spot emits spatially uncorrelated TLSs. Hence, the spatio-temporal structure of the light emitted can be shaped by individually addressing the pulses emitted by each spot. Because the maximum number of pulses circulating in the cavity and the number of positive net-gain spots in the VECSEL can be increased straightforwardly, this result is a proof of concept of a laser platform capable of handling light states of scalable complexity. We discuss applications to three dimensional all-optical buffer and to multiplexing of frequency combs that share the same laser cavity.

1. Introduction

The possibility of controlling the spatio-temporal structure of light is one of the main challenges of modern photonics [1–4]. A variety of spatially complex, though stationary, light states have been demonstrated in degenerate laser cavities [5,6] by using an intracavity spatial light modulator [7,8], metasurfaces [9,10] and through the generation of spatial Localized Structures [11–14]. Localized Structures, also called dissipative solitons, are individually addressable structures which appear in large aspect-ratio resonators [15–18]. Because they can be used for encoding information bits, LS have been proposed for a variety of applications to information processing [19–22]. More recently, the concept of Localized Structures has been extended to the time domain; temporal Localized Structures (TLSs) are addressable pulses which, exactly as their spatial counterparts, can be used as data bits for all-optical buffers and, more generally, as fundamental bricks for shaping the temporal structure of a light beam [23–28]. TLSs are also deeply related to the generation of frequency combs [29, 30].

Despite these significant progresses, the control of the *spatio-temporal* structure of light is only at its beginning. Spatio-temporal mode locking states were recently reported in optical fibers [31, 32] and temporally localized Turing patterns have been observed in a degenerate cavity Vertical External-Cavity Surface-Emitting Lasers (VECSEL) with an intracavity saturable absorber [33].

III-V semiconductor based VECSELs are promising platforms for generating spatio-temporal light states because they can gather together a large aspect-ratio cavity and the ingredients for temporal LS. While the former requires a nearly self-imaging (SI), i.e. degenerate, external-cavity and a broad-area pumping, the latter is achieved in the limit of cavity round-trip (τ) larger than the gain recovery time (τ_g) ($\tau > \tau_g$) and for a large modulation depth saturable absorber mirror [24, 34].

In this paper we show that a degenerate cavity VECSEL operated in the regime of TLSs can be engineered to generate light with a reconfigurable spatio-temporal structure. Spatial shaping is obtained by depositing an absorptive and non-diffractive Chromium mask on the top of the gain section. This mask can be drawn in an arbitrary shape and it modulates the losses in the transverse plane of the cavity accordingly [9, 35]. In order to provide a proof of concept of spatio-temporal control of light, we draw a positive net-gain landscape in the form of two separate round spots (*hot-spots* from now on). We show that each one of these spots behaves as an independent source of TLSs and we demonstrate spatially selective addressing of individual pulses traveling into the cavity. By controlling the number of pulses per roundtrip emitted by each spot, which ranges from zero (no emission) to a maximum value (N_{max}) determined by the ratio τ/τ_g, the VECSEL light emission can be customized in a large number of different spatio-temporal states.

Our realization paves the way towards an all-optical buffer where information bits can be stored in the three dimension of the resonator. Moreover, because each hot-spot emits a frequency comb, we obtain a double frequency comb sharing the same laser medium and cavity [36–38]. Finally, we point out that the complexity of the light states generated by the described VECSEL scales with the number of the hot-spots inserted and with the length of the resonator, which can be both increased straightforwardly. These developments and their impact on applications are discussed.

2. Experimental Set-up

The VECSEL has a L-shaped self-imaging cavity delimited by the gain mirror (also called 1/2 VCSEL) and by a saturable absorber mirror (see Fig. 1). VECSEL's elements are based on III-V semiconductor technology. The gain mirror is fabricated on a GaAs substrate with 12 strain-balanced InGaAs/GaAsP quantum wells (QWs) designed for barrier optical pumping and emitting at 1.06 μm. It is optically pumped at 808 nm by a flat-top elliptical profile having an horizontal axis of 90 μm and a vertical one of 50 μm. The SESAM features a single strained InGaAs/GaAs QW located near the external surface leading to recombination rate approximately two orders of magnitudes faster than the gain medium. The saturated/unsaturated reflectivity modulation depth (ΔR) of the SESAM must exceed a critical value (typically $\Delta R > 8\%$, [34]) for operating the VECSEL in the TLS regime. This parameter can be varied by tuning the gain mirror and the SESAM microcavities resonances (λ_G and λ_{SA} respectively) and, in the experiment here described, we fixed $\delta\lambda = \lambda_{SA} - \lambda_G = 8\ nm$, leading to $\Delta R \approx 15\%$.

The degenerate external cavity is designed to be long enough to fulfill the condition for achieving the TLS regime ($\tau \approx 4.2\,ns > \tau_g \approx 1\,ns$). Moreover, SESAM and gain mirror are placed in conjugate planes with a magnification factor of two for increasing effectively the ratio between gain and SESAM saturation fluences. More details on VECSEL's components and on the design of SI external cavity can be found in [33]. The VECSEL's output beam is sent to the detection part where the far-field and near-field profiles are imaged on two CCD cameras. The near-field is also imaged on an array of optical fibers for spatially resolved detection at 10 GHz bandwidth (34 GHz for pulse width measurements).

A $5 - 10\,nm$ thick highly absorptive (> 90% at 1.06 μm) metallic (Cr) layer has been deposited on top of the gain structure. Thanks to e-beam lithographic post-growth process and lift-off, the shape of this layer can be arbitrarily drawn with a 5 nm spatial resolution, hence generating a non-diffractive mask which modulates the net optical gain in the transverse plane of the VECSEL (Fig. 1 panel c). A large number of masks having different shapes and pattern geometries

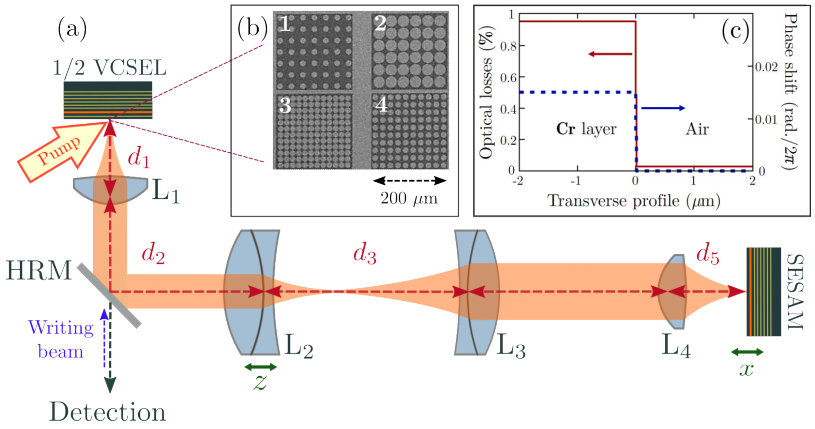

Fig. 1. a) Experimental set-up showing the L-shape VECSEL. HRM= high reflectivity beam splitter (> 99.5% at 1.060 nm). L_i are lenses whose focal lengths are $f_1 = f_4 = 8\ mm$, $f_2 = 200\ mm$, $f_3 = 100\ mm$. While in cold cavity SI condition is reached for telescopic arrangement of optical elements, the presence of a thermal lens [39] due to optical pump beam ($f_{th} \approx \frac{10\ mm\ W}{P_p}$,) requires slight correction to telescopic arrangement to achieve degenerate condition. Accordingly, distances for SI condition are: d_1 (gain section/L_1) = f_1; d_2 (L_1/L_2)=f_1+f_2 + z_0; d_3 (L_2/L_3)=f_1+f_2 − z_0; d_4 (L_3/L_4)=f_3+f_4; d_5 (L_4/SESAM)=f_4 + x_0, where $z_0 = -\frac{f_c^2}{2f_{th}}$ and $x_0 = -\frac{f_c^4}{2M^2 f_2^2 f_{th}}$. For typical pump power values used in our experiment ($P_p \approx 170\ mW$) $f_{th} \approx 60\ mm$: $z_0 \approx 0.53\ mm$ and $x_0 \approx 0.8\ \mu m$ [33]. b): Microscope pictures of some of the masks deposited onto the gain mirror. The darker zones correspond to Cr layer that provides losses larger than 90%. The masks shown exhibit arrangements of circular holes where the absorptive material has been removed. Diameters of holes (D) and separation between centers (T) are $D = 15\ \mu m$, $T = 30\ \mu m$ in mask 1, $D = 30\ \mu m$, $T = 32\ \mu m$ in mask 2, $D = 15\ \mu m$, $T = 16\ \mu m$ in mask 3, $D = 15\ \mu m$, $T = 20\ \mu m$ in mask 4. c) Transverse profile of the losses and of the phase shift experienced by the electromagnetic field when reflected by the gain mirror around Cr mask borderline. The Cr edge has less than 5nm rising thickness. The phase shift of the mask is less than $2\pi/50$.

have been drawn on the gain sample. Each mask has a size of $200X200\ \mu m$ and, by shifting transversely the gain sample in front of the optical pump beam, different net-gain landscapes can be studied using the same VECSEL cavity. In this paper we analyze the effect on the VECSEL emission of a net-gain landscape composed by circular spots (*hot-spots*) with sharp sub-wavelength edges, as the ones shown in Fig. 1, panel b). The presence of these masks on the gain section increases dramatically the total amount of losses in the VECSEL cavity and lasing emission has been obtained only in presence of hot-spots having a diameter of at least 15 μm. However, we have used hot-spots having a diameter of 30 μm for reaching output levels strong enough to ensure a good noise to signal ratio from our fast detectors. We choose the mask with the highest density of circles (32 μm distance between their centers, Mask 2 in Fig. 1b) and, accordingly, two hot-spots fit in the pumped area.

3. Experimental Results

The VECSEL spatio-temporal emission is described in Fig. 2. The near-field and far-field time averaged profiles reveal that each hot-spot emits a couple of tilted beams whose transverse wavevectors have the module and opposite direction ($\pm\vec{k_t}$). The interference of the two beams generates a stripe pattern in the near-field profile at each spot. Tilted beams emission is typical of

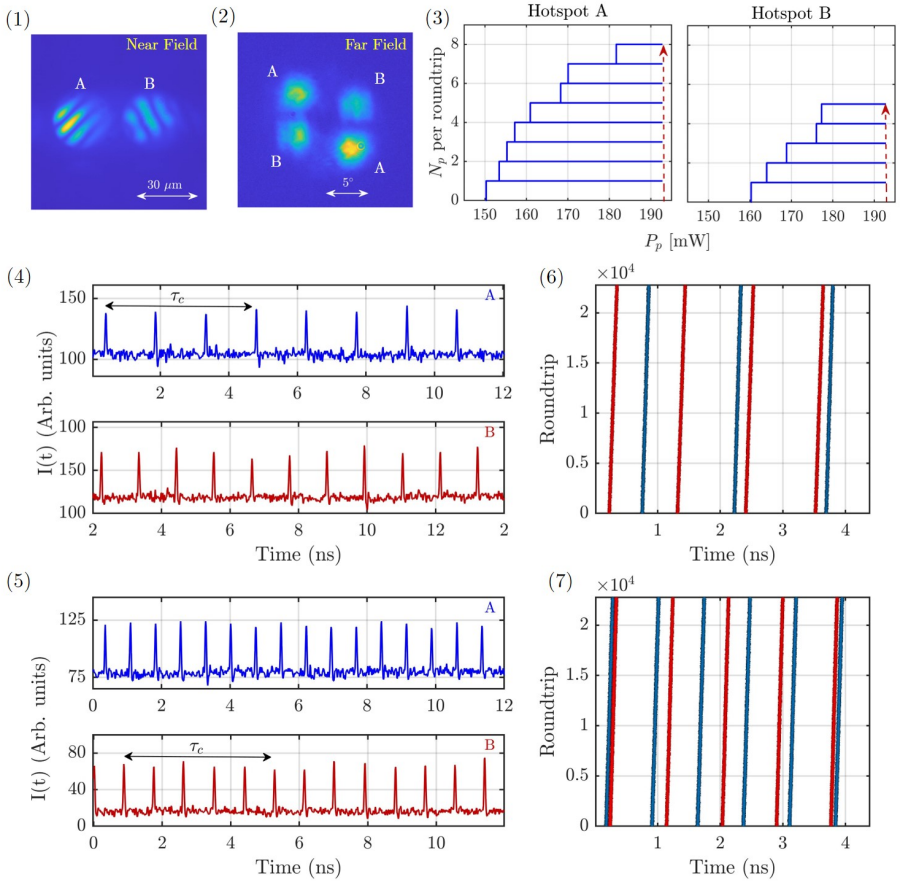

Fig. 2. Spatio-temporal behavior of the light emitted by the VECSEL with two hot-spots in the gain section (A and B). In panel 1) and 2) we show the time-averaged near-field and far-field profiles of the VECSEL emission. In panel 3) we show the bifurcation diagrams of the mode-locking emission from each hot-spot. These diagram are obtained according to the following procedure : pump power P_p is increased from zero up to the VECSEL threshold value ($P_{p,th}$ = 192.5 mA), where off solution becomes unstable at the advantage of a mode-locked emission having N_{max} pulses per roundtrip. Then, P_p is decreased until the emission jumps to the emission having $N_{max} - 1$ pulses per roundtrip. At this point the stability of this solution is tested by increasing again P_p up to $P_{p,th}$ and by decreasing it down to the point where the emission jumps to the solution with $N_{max} - 2$ pulses per roundtrip. This is repeated for every solution with a number of pulses per roundtrip different from zero, until the system jumps to the off solution. The difference in the number N_{max} pulses per roundtrip for the two hot-spots is due to a non perfectly homogeneous level of pumping of the two regions. In panels 4 and 5 we show two different emission states obtained for the same parameter values in the multistable region (P_p = 185 mW). The blue (red) time trace represents the intensity emitted by hot-spot A (B). In panel 4) we show the state (N_A=3, N_B=4) while in panel 5) we show the state (N_A=6, N_B=5). Space-time diagrams of these states, picturing the evolution of the pulses emitted roundtrip after roundtrip, are represented in panels 6) (N_A=3, N_B=4) and 7) (N_A=6, N_B=5).

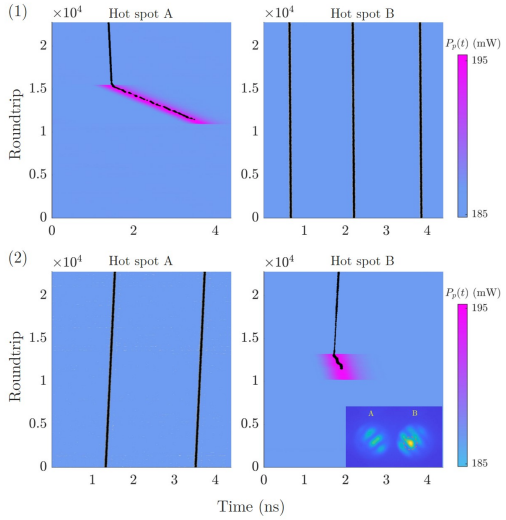

Fig. 3. Space-time diagram of the writing process of TLS in each hot-spot. (a) Writing of one LS in the hot-spot A while hot-spot B is emitting three TLSs per roundtrip ($N_B = 3$). The writing pump pulse is applied at the round-trip #10000 and spot A emits a TLS which follows the timing of the perturbation pulse which is incidentally different from the roundtrip of the system. When the writing pulse is removed at the round-trip #15500, the solution $N_A = 1$ remains stable. b) Writing of one TLS in the hot-spot B while hot-spot A is emitting $N_A = 2$ TLS per roundtrip. In the inset we show the time-averaged near-field emission of the VECSEL during the application of the perturbation to hot-spot B. The waist of the perturbation beam can be compared with the interference fringes.

degenerate cavities [40–42] and it is related to spherical aberrations of the optical elements of the cavity, which become more and more relevant close to SI conditions. Moreover, the interference pattern in the near-field enable an effective saturation of the SESAM. It is worth noting that the direction of the transverse wave-vectors can be different for each spot. In the situation shown in Fig. 2, the two hot-spots emit beams which are in orthogonal directions, thus allowing separation of the two emissions both in near and far-field. Slight tilting of the optical elements enables some control on these directions. The direction of the tilted beams emitted by a hot-spot can be imposed by introducing some ellipticity in the hot-spot shape, thus breaking the azimuthal symmetry and forcing a well determined direction $\pm\overrightarrow{k_t}$.

The analysis of the VECSEL emission in the time domain reveals that each spot emits mode-locked solutions with a number of pulses per round-trip (N_A and N_B) which can be varied by changing the pump value, as shown in Fig. 2, panel 3. These stability diagrams reveals that each hot-spot feature multi-stability between different mode-locked states with number of pulses per round-trip ranging between N_A=0 (no emission) to $N_{A,max}$=8 and between N_B=0 (no emission) to $N_{B,max}$=5. This multi-stability is a signature of temporally localized structures which, in our VECSELs, are emitted by two spatially independent hot-spots. In the multistable range, $160\,mW < P_p < 190\,mW$, different combinations of N_A and N_B can be obtained in the VECSELs emission simply by perturbing the system. This can be done by opening and closing the light path inside the cavity. Two examples of these combinations are given in Fig. 2, panel 4) and 6) where N_A=3, N_B=4 and in panel 5) and 7) where N_A=6, N_B=5. The duration of the pulses cannot be resolved by our detection bandwidth, hence pulse with is smaller than 20 ps. Time-averaged output power from each spot is about 20 μW

These experimental evidences show that a degenerate cavity can host two spatially decorrelated sources of TLSs emitting beams with different transverse wave-vectors, thus providing spatio-temporally structured light. In addition, because TLS are individually addressable pulse, we can control the number of pulses emitted by each spot by perturbing locally the pump intensity. This control is achieved by injecting a short pump pulse having a waist of only 7 μm,thus targeting a single hot-spot. The system is prepared in the multistable parameter region and the amplitude of the addressing pump pulse is chosen to bring the system beyond the upper limit of the multistable region ($P_p > 190\, mW$). This perturbation is applied synchronously with the cavity roundtrip for about one thousand roundtrips. In Fig. 3 a) we demonstrate the addressing of a pulse emitted by hot-spot A starting from the initial condition where N_A= 0, N_B = 3. This process is illustrated by using a space-time diagram where the writing pump pulse is represented with a color scale, while the trajectory of each emitted pulse is represented by a black trace. The writing pulse is applied at the round-trip 10000 and it is sufficiently short to switch on a single temporal LS. The written pulse persists after the perturbation is removed. It is worth noting that no effect is produced onto the emission from hot-spot B during and after the writing process. In Figure 3 b) we repeat the operation by targeting the hot-spot B starting from the initial condition $N_A = 2$ and $N_B = 0$. Other initial conditions can be chosen with similar results, provided that the addressing pulse is separated in time from the preexisting LS of at least τ_g. Pulse erasure is also obtained by perturbing a single hot-spot with a negative pump pulse, as done in [33].

4. Discussion

This result provides a demonstration of a laser source capable of generating spatio-temporally structured light beams organized on two spatial channels and on a number of pulses in each channel ranging from zero to 5 in hot-spot A, and from zero to 8 in hot-spot B. If we identify light states simply by the number of pulses emitted by each hot-spot (N_A, N_B), the number of different light states that can be obtained is 54. In general, if we consider that the value of N_{max} is the same for all the hot-spots, the number of combinations in a VECSEL with n hot-spots is given by $(N_{max} + 1)^n$. The maximum number of TLS per channel (N_{max}) depends on the ratio between cavity roundtrip and gain recovery time (τ/τ_g) [24] which can be increased straightforwardly by using longer resonators. On the other hand, there are no technological obstacles to increase n up to eight by doubling the optical pump size. For larger sizes, the total pump power will exceed 1 W and thermal management solutions of the gain section will be necessary. These solutions require additional technological steps in the realization of the gain mirror as, for example, integration of a diamond heat spreader. These considerations reveal that the demonstrated laser platform is capable of handling light states of scalable complexity.

The generated light states are particularly suitable for applications to information processing, since each pulse circulating in the cavity can be used to encode an information bit. Accordingly, the VECSEL described in this paper can be used as an all-optical buffer whose memory size is given by the product $n \cdot N_{max}$. Another possible application is related to the use of each hot-spot as a source of a frequency comb. Accordingly, the VECSEL laser described enables multiplexing of frequency combs sharing the same active/passive medium, i.e. the same noise sources, thus increasing the mutual coherence required for multi-frequency comb operations [36–38]. Moreover, the possibility of varying the comb tooth spacing of each hot-spot by addressing the number of pulses per roundtrip emitted, provides an additional degrees of freedom for controlling the spectral line density of the resulting RF comb.

The evolution of the TLSs roundtrip after roundtrip, shown in Fig. 2 panels 6) and 7), reveals that the periodicity of the TLS is the same for both hot-spots regardless the number of pulses emitted per roundtrip, in contrast to previous observations in TLS emitters with homogeneous net-gain profile [26]. Then, a form of synchronization between the two hot-spots takes place in our VECSEL due to the fact that they share the same active and passive media. This period

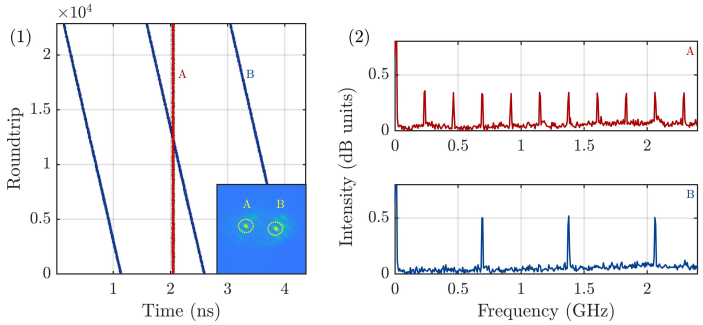

Fig. 4. Panel a) Evolution of the TLS emitted by hot-spot A (red trace) and B (blue trace) in presence of two continuous wave (CW) 7 μm-waist pump beams targeting the hot-spots A and B. Their powers P_A and $P_B$can be controlled independently. Here P_A= 35 mW and P_B= 45 mW. Both narrow waist pump beamb are superimposed to the homogeneous pump beam which is kept to a power P_p= 120 mW. Inset: Near-field time-averaged emission of the VECSEL showing the presence of the two 7 μm-waist independent pumps targeting hot-spots A and B. Panel 2) Power spectra of the two outputs from hot-spot A (red trace) and B (blue trace)

locking has been observed for different combinations of N_A and N_B and it persists in emission states where the difference between N_A and N_B is maximized (| N_A−N_B |= 4).

This phenomenon is beneficial for data buffering since a common clock can be established for all the channels of the buffer. On the other hand, for multi frequency combs generation, it is required that the pulse trains emitted by the two hot-spots have incommensurate repetition rates. This can be obtained by controlling locally the continuous wave (CW) pump power impinging each hot-spot. To this aim, we superpose to the homogeneous pump two pump beams having a waist of 7 μm and whose power, P_A and P_B, can be controlled independently. Thanks to the multistable response of the VECSEL, an arbitrary emission state (N_A, N_B) is robust upon variation of P_A and P_B in the interval where the states N_A and N_B are stable (see Fig. 2 panel 3)). Because the repetition rate of the emitted TLS depends on the pumping level, the local pump power P_A (P_B) enables to tune slightly the period $\tau_A(\tau_B)$ of the TLS emitted by hot-spot $A(B)$ [26]. In Fig. 4 we have set the emission state N_A=1, N_B = 3 and we have induced a difference between τ_A and τ_B by increasing P_A over P_B. This difference is evident in the space-time diagram of Fig. 4, showing the walk-off of the pulses emitted by hot-spot B versus the pulse emitted by hot-spot A. This walk off is approximately 1 ns after 22500 roundtrips , thus leading to | τ_A− τ_B | = 4.4 10^{-5} ns. Accordingly, the combination of the frequency combs generated by hot-spots A and B leads to a RF spectrum having lines separated by Δf_r =|1/τ_A-1/τ_B |= 2.5 kHz. The full characterization of this double frequency comb is out of the scope of this manuscript and it will be presented elsewhere.

In conclusion, we have shown that degenerate III-V semiconductor VECSELs with an intracavity saturable absorber are promising platform for generating light with an addressable spatio-temporal structure. Control of spatial profile relies on the introduction of two spots of positive net-gain onto the gain section, while temporal control of light is obtained thanks to the properties of TLSs. By controlling the number of pulses emitting by each spot, the light emitted can be reconfigured in a large variety of different spatio-temporal states. Because each pulse can be used to encode an information bit, the VECSEL described materializes an all-optical three dimensional buffer. Moreover, we have shown that each spot can be used as a frequency comb source, thus leading to a double frequency comb in the same laser cavity. These proof of concepts are based on two spatial channels and a small number of pulses per roundtrip, however

these figures can be increased straightforwardly by increasing the size of the pump and the length of the cavity.

5. Backmatter

Funding. The INPHYNI Group acknowledges project ANR-18-CE24-0002 BLASON and funding of Région PACA OPTIMAL.).

Acknowledgements. This work was supported by the French RENATECH network.

Disclosures. The authors declare no conflicts of interest.

References

1. A. Forbes, M. de Oliveira, and M. Dennis, "Structured light," Nat. Photonics pp. 253–262 (2021).
2. M. Piccardo, V. Ginis, A. Forbes, S. Mahler, A. A. Friesem, N. Davidson, H. Ren, A. H. Dorrah, F. Capasso, F. T. Dullo, B. S. Ahluwalia, A. Ambrosio, S. Gigan, N. Treps, M. Hiekkamäki, R. Fickler, M. Kues, D. Moss, R. Morandotti, J. Riemensberger, T. J. Kippenberg, J. Faist, G. Scalari, N. Picqué, T. W. Hänsch, G. Cerullo, C. Manzoni, L. A. Lugiato, M. Brambilla, L. Columbo, A. Gatti, F. Prati, A. Shiri, A. F. Abouraddy, A. Alù, E. Galiffi, J. B. Pendry, and P. A. Huidobro, "Roadmap on multimode light shaping," J. Opt. **24**, 013001 (2021).
3. L. G. Wright, W. H. Renninger, D. N. Christodoulides, and F. W. Wise, "Nonlinear multimode photonics: nonlinear optics with many degrees of freedom," Optica. **9**, 824–841 (2022).
4. N. Davidson, S. Mahler, A. Friesem, and A. Forbes, "Complex-light lasers," Opt. Photon. News **33**, 26–33 (2022).
5. H. Cao, C. R., S. Bittner, and al., "Complex lasers with controllable coherence," Nat. Rev. Phys. **1**, 156–158 (2019).
6. S. Knitter, C. Liu, B. Redding, M. K. Khokha, M. A. Choma, and H. Cao, "Coherence switching of a degenerate vecsel for multimodality imaging," Optica. **3**, 403–406 (2016).
7. C. Tradonsky, S. Mahler, G. Cai, V. Pal, R. Chriki, A. A. Friesem, and N. Davidson, "High-resolution digital spatial control of a highly multimode laser," Optica. **8**, 880–884 (2021).
8. S. Ngcobo, I. Itvine, L. Burger, and A. Forbes, "A digital laser for on-demand laser modes," Nat. Commun. p. 2289 (2013).
9. M. S. Seghilani, M. Myara, M. Sellahi, L. Legratiet, I. Sagnes, G. Beaudoin, P. Lalanne, and A. Garnache, "Vortex laser based on iii-v semiconductor metasurface: direct generation of coherent laguerre-gauss modes carrying controlled orbital angular momentum," Sci. Reports **6**, 38156 EP – (2016). Article.
10. M. Piccardo, M. de Oliveira, A. Toma, V. Aglieri, A. Forbes, and A. Ambrosio, "Vortex laser arrays with topological charge control and self-healing of defects," Nat. Photonics pp. 359–365 (2022).
11. S. Barland, J. R. Tredicce, M. Brambilla, L. A. Lugiato, S. Balle, M. Giudici, T. Maggipinto, L. Spinelli, G. Tissoni, T. Knödl, M. Miller, and R. Jäger, "Cavity solitons as pixels in semiconductor microcavities," Nature **419**, 699–702 (2002).
12. Y. Tanguy, T. Ackemann, W. J. Firth, and R. Jäger, "Realization of a semiconductor-based cavity soliton laser," Phys. Rev. Lett. **100**, 013907 (2008).
13. P. Genevet, S. Barland, M. Giudici, and J. R. Tredicce, "Cavity soliton laser based on mutually coupled semiconductor microresonators," Phys. Rev. Lett. **101**, 123905 (2008).
14. P. Genevet, S. Barland, M. Giudici, and J. R. Tredicce, "Bistable and addressable localized vortices in semiconductor lasers," Phys. Rev. Lett. **104**, 223902 (2010).
15. N. N. Rosanov and G. V. Khodova, "Autosolitons in nonlinear interferometers," Opt. Spectrosc. **65**, 449–450 (1988).
16. L. Lugiato, "Introduction to the feature section on cavity solitons: An overview," Quantum Electron. IEEE J. **39**, 193–196 (2003).
17. P. Mandel and M. Tlidi, "Transverse dynamics in cavity nonlinear optics (2000–2003)," J. Opt. B: Quantum Semiclassical Opt. **6**, R60 (2004).
18. T. Ackemann, W. J. Firth, and G. Oppo, "Chapter 6 fundamentals and applications of spatial dissipative solitons in photonic devices," in *Advances in Atomic Molecular and Optical Physics,* , vol. 57 of *Advances In Atomic, Molecular, and Optical Physics* P. R. B. E. Arimondo and C. C. Lin, eds. (Academic Press, 2009), pp. 323 – 421.
19. P. Coullet, C. Riera, and C. Tresser, "A new approach to data storage using localized structures," Chaos. **14**, 193–201 (2004).
20. F. Pedaci, P. Genevet, S. Barland, M. Giudici, and J. R. Tredicce, "Positioning cavity solitons with a phase mask," Appl. Phys. Lett. **89**, 221111 (2006).
21. F. Pedaci, G. Tissoni, S. Barland, M. Giudici, and J. R. Tredicce, "Mapping local defects of extended media using localized structures," Appl. Phys. Lett. **93**, 111104 (2008).
22. F. Pedaci, S. Barland, E. Caboche, P. Genevet, M. Giudici, J. R. Tredicce, T. Ackemann, A. J. Scroggie, W. J. Firth, G.-L. Oppo, G. Tissoni, and R. Jäger, "All-optical delay line using semiconductor cavity solitons," Appl. Phys. Lett. **92**, 011101 (2008).
23. F. Leo, S. Coen, P. Kockaert, S. Gorza, P. Emplit, and M. Haelterman, "Temporal cavity solitons in one-dimensional kerr media as bits in an all-optical buffer," Nat Photon **4**, 471–476 (2010).

24. M. Marconi, J. Javaloyes, S. Balle, and M. Giudici, "How lasing localized structures evolve out of passive mode locking," Phys. Rev. Lett. **112**, 223901 (2014).
25. M. Marconi, J. Javaloyes, S. Barland, S. Balle, and M. Giudici, "Vectorial dissipative solitons in vertical-cavity surface-emitting lasers with delays," Nat. Photonics **9**, 450–455 (2015).
26. P. Camelin, J. Javaloyes, M. Marconi, and M. Giudici, "Electrical addressing and temporal tweezing of localized pulses in passively-mode-locked semiconductor lasers," Phys. Rev. A **94**, 063854 (2016).
27. S. Barland, S. Coen, M. Erkintalo, M. Giudici, J. Javaloyes, and S. Murdoch, "Temporal localized structures in optical resonators," Adv. Physics: X **2**, 496–517 (2017).
28. N. Englebert, C. Mas-Arabi, P. Parra-Rivas, S. Gorza, and F. Leo, "Temporal solitons in a coherently driven active resonator," Nat. Photonics. **15**, 536–541 (2021).
29. T. Herr, V. Brasch, J. D. Jost, C. Y. Wang, N. M. Kondratiev, M. L. Gorodetsky, and T. J. Kippenberg, "Temporal solitons in optical microresonators," Nat. Photonics **8**, 145–152 (2014).
30. A. Bao, Hualongand Cooper, M. Rowley, L. Di Lauro, J. S. Totero Gongora, S. T. Chu, B. E. Little, G.-L. Oppo, R. Morandotti, D. J. Moss, B. Wetzel, M. Peccianti, and A. Pasquazi, "Observation of mode-locked spatial laser solitons," Nat. Photonics. **13**, 384–389 (2019).
31. L. G. Wright, D. N. Christodoulides, and F. W. Wise, "Spatiotemporal mode-locking in multimode fiber lasers," Science. **358**, 94–97 (2017).
32. L. G. Wright, P. Sidorenko, H. Pourbeyram, Z. M. Ziegler, A. Isichenko, B. A. Malomed, C. R. Menyuk, D. N. Christodoulides, and F. W. Wise, "Mechanisms of spatiotemporal mode-locking," Nat. Phys. **16**, 565–270 (2020).
33. A. Bartolo, N. Vigne, M. Marconi, G. Beaudoin, K. Pantzas, I. Sagnes, G. Huyet, F. Maucher, S. V. Gurevich, J. Javaloyes, A. Garnache, and M. Giudici, "Temporal localized turing patterns in mode-locked semiconductor lasers," Optica. **9**, 1386–1393 (2022).
34. P. Camelin, C. Schelte, A. Verschelde, A. Garnache, G. Beaudoin, I. Sagnes, G. Huyet, J. Javaloyes, S. Gurevich, and M. Giudici, "Temporal localized structures in mode-locked vertical external-cavity surface-emitting laser," Opt. Lett. **43**, 5367 (2018).
35. S. Blin, R. Paquet, M. Myara, B. Chomet, L. Le Gratiet, M. Sellahi, G. Beaudoin, I. Sagnes, G. Ducournau, P. Latzel, J.-F. Lampin, and A. Garnache, "Coherent and tunable thz emission driven by an integrated iii–v semiconductor laser," IEEE J. Sel. Top. Quantum Electron. **23**, 1–11 (2017).
36. I. Coddington, N. Newbury, and W. Swann, "Dual-comb spectroscopy," Optica. **3**, 414–426 (2016).
37. S. M. Link, A. Klenner, M. Mangold, C. A. Zaugg, M. Golling, B. W. Tilma, and U. Keller, "Dual-comb modelocked laser," Opt. Express **23**, 5521–5531 (2015).
38. J. Pupeikis, B. Willenberg, S. L. Camenzind, A. Benayad, P. Camy, C. R. Phillips, and U. Keller, "Spatially multiplexed single-cavity dual-comb laser," Optica **9**, 713–716 (2022).
39. A. Laurain, M. Myara, G. Beaudoin, I. Sagnes, and A. Garnache, "High power single–frequency continuously–tunable compact extended–cavity semiconductor laser," Opt. Express **17**, 9503–9508 (2009).
40. X. Hachair, S. Barbay, T. Elsass, I. Sagnes, and R. Kuszelewicz, "Transverse spatial structure of a high fresnel number vertical external cavity surface emitting laser," Opt. Express **16**, 9519–9527 (2008).
41. A. A. Bartolo González, "Spatial organization of localized pulses in a self-imaging vertical external cavity surface emitting laser," Theses, Université Côte d'Azur (2022).
42. S. Gurevich, F. Maucher, N. Vigne, A. A. Bartolo, M. Marconi, G. Beaudoin, K. Pantzas, I. Sagnes, A. Garnache, M. Giudici, and J. Javaloyes, "Quartic beams of temporal solitons in a nearly-degenerated laser cavity," Submitt. to Nat. Photonics .